Monthly Notices
of the
ROYAL ASTRONOMICAL SOCIETY

MNRAS **469,** 1117–1130 (2017)
Advance Access publication 2017 April 12

doi:10.1093/mnras/stx897

Hydrodynamic ablation of protoplanetary discs via supernovae

J. L. Close★ and J. M. Pittard

School of Physics and Astronomy, University of Leeds, Leeds LS2 9JT, UK

Accepted 2017 April 10. Received 2017 March 30; in original form 2016 September 26

ABSTRACT

We present three-dimensional simulations of a protoplanetary disc subject to the effect of a nearby (0.3 pc distant) supernova (SN), using a time-dependent flow from a one-dimensional numerical model of the supernova remnant (SNR), in addition to constant peak ram pressure simulations. Simulations are performed for a variety of disc masses and inclination angles. We find disc mass-loss rates that are typically 10^{-7}–10^{-6} $M_{\odot}$ yr^{-1} (but they peak near 10^{-5} $M_{\odot}$ yr^{-1} during the 'instantaneous' stripping phase) and are sustained for around 200 yr. Inclination angle has little effect on the mass-loss unless the disc is close to edge-on. Inclined discs also strip asymmetrically with the trailing edge ablating more easily. Since the interaction lasts less than one outer rotation period, there is not enough time for the disc to restore its symmetry, leaving the disc asymmetrical after the flow has passed. Of the low-mass discs considered, only the edge-on disc is able to survive interaction with the SNR (with 50 per cent of its initial mass remaining). At the end of the simulations, discs that survive contain fractional masses of SN material up to 5×10^{-6}. This is too low to explain the abundance of short-lived radionuclides in the early Solar system, but a larger disc and the inclusion of radiative cooling might allow the disc to capture a higher fraction of SN material.

Key words: hydrodynamics – methods: numerical – protoplanetary discs – ISM: supernova remnants.

1 INTRODUCTION

It is widely believed that massive stars can trigger the formation of lower mass stars in their surrounding regions, leading to frequent associations of massive stars, and young low-mass stars. For instance, there are ∼2000 low-mass stars within 2 pc of the centre of the Trapezium cluster (Hillenbrand & Hartmann 1998), and stars with circumstellar discs (O'dell, Wen & Hu 1993; McCaughrean & O'dell 1996; Bally et al. 1998) within a few tenths of a parsec of the central star, θ^1 Ori C. As massive stars are often the source of strong winds, high ionizing radiation flux and eventual supernovae (SNe), these regions are potentially hostile to protoplanetary discs and the subsequent formation of planets. The interactions massive stars have with other stars and their discs can be broadly categorized into gravitational, radiation or ablation.

When two stars pass one another, the associated discs become perturbed by the gravitational interaction. If this interaction is strong enough, material from the disc can become unbound (Clarke & Pringle 1993). Scally & Clarke (2001) use *N*-body simulations to model the dynamics of the stars in the Orion Nebula. They find that only a small fraction of the stars interact closely on the expected disc dispersal time-scales, and so close encounters are not a major contributor to protoplanetary disc dispersal.

Direct observational evidence of the effects of radiation on discs is seen in the form of the proplyds in the Orion Nebula (e.g. O'dell & Wen 1994; McCaughrean 2001). The radiation from θ^1 Ori C causes a photoevaporation flow from the discs, which collides with the oncoming stellar wind. This results in a number of cometary-shaped ionization fronts associated with stars around θ^1 Ori C. Estimates put the mass-loss rate of the proplyds at $\sim 4 \times 10^{-7}$ $M_{\odot}$ yr^{-1} (Henney & O'Dell 1999). If sustained over the lifetime of the cluster, this would mean that the stars would have had unrealistically massive discs (greater than the star's mass) at some point in the past. However, θ^1 Ori C may have switched on only $\sim 10^5$ yr ago (Scally & Clarke 2001), in which case it is unlikely that the combination of photoevaporation and viscous accretion will have significantly depleted the discs (Garcia 2011). This suggests that the Orion Nebula is in a relativity short-lived stage of its evolution, which is consistent with the lack of proplyd-like objects in other clusters (e.g. Stapelfeldt et al. 1997; Balog et al. 2006).

There is now a lot of observational evidence that massive stars influence the discs of neighbouring stars. Cometary tails are seen to extend from protoplanetary discs in *Hubble Space Telescope* images of the Orion Nebula (e.g. Smith et al. 2005; Ricci, Robberto & Soderblom 2008), while sub-millimetre observations of the Trapezium Cluster reveal that discs within a few tenths of a parsec of θ^1 Ori C are truncated (Mann & Williams 2009, 2010; Mann et al. 2014). However, the degree to which massive stars affect nearby discs remains uncertain. For instance, Mann et al. (2015) claim that there is

★ E-mail: py08jlc@leeds.ac.uk

no evidence for disc truncation in the Flame Nebula (NGC 2024), though it is somewhat younger and hosts a less massive star compared to the Trapezium cluster. In addition, Richert et al. (2015) argue that there is no evidence for the depletion of the inner discs around pre-main-sequence stars in the vicinity of O-type stars, even very luminous O2–O5 stars. In contrast, Povich et al. (2016) claim that rapid disc evolution on <1 Myr time-scales has produced a significant population of intermediate-mass pre-main-sequence stars lacking inner dust discs.

Likewise, significant differences in the mass-loss rate and lifetime of discs exist in theoretical studies of their photoevaporation. Some studies claim lifetimes of only 10^5 yr (e.g. Johnstone, Hollenbach & Bally 1998; Störzer & Hollenbach 1999), substantially shorter than the 10^6–10^7 yr lifetime of discs subject only to viscous accretion (Haisch, Lada & Lada 2001; Hernández et al. 2007, and references therein). In contrast, a recent model combining viscous accretion and external photoevaporation predicts that disc lifetimes are shortened by only a factor of a few (Anderson, Adams & Calvet 2013). In addition, if the outer parts of the disc can be totally removed, the inner disc may rapidly disappear if it is starved of material needed to offset accretion on to the star (Anderson et al. 2013). Thus, the significance of external photoevaporation on disc lifetimes remains highly uncertain.

Supernova remnants (SNRs) provide another source of agitation for protoplanetary discs. There is evidence in π Sco of circumstellar discs similar to those in the Orion Nebula (Bertoldi & Jenkins 1992) that an SN occurred nearby $\sim 10^6$ yr ago (de Geus 1992). Lada & Lada (2003) compiled a catalogue of embedded clusters and find that the vast majority (70–90 per cent) of stars form in clusters of >100 members, and the majority of those (~ 75 per cent) are in clusters containing stars massive enough to give rise to SNe (Hester & Desch 2005).

Analytic estimates for the ablation of protoplanetary discs due to an SNR were presented by Chevalier (2000). He found that for typical disc and SN parameters, partial stripping of the disc can occur, but typically not its complete disruption. This suggests that although the discs are affected, they can survive such events.

The interaction of an SNR with a protoplanetary disc is also of interest from the point of view of injecting short-lived radionuclides (SLRs) into the early Solar system (e.g. Cameron & Truran 1977; Jacobsen 2005; Looney, Tobin & Fields 2006). Analyses of meteorites suggest that the early Solar system had a higher abundance of SLRs than the average interstellar medium value (see e.g. Diehl et al. 2006, for ^{26}Al). This means that the SLRs must have been injected into the Solar system at some point during its history, and due to the short half-life of ^{60}Fe (Rugel et al. 2009, 2.6 Myr), this constrains the injection event to a time close to the Solar system's formation. Given that SNe are abundant sources of nucleosynthesis and they are often in close proximity to young, low-mass stars, they are seen as a good candidate for the source of SLRs in the early Solar system. While some SLRs can be explained by production internal to the Solar system, ^{60}Fe is practically impossible to produce locally (Lee et al. 1998; Gounelle et al. 2006).

If the formation of the Solar system was triggered by an SNR, this could provide a source of SLRs (see e.g. Foster & Boss 1996; Boss & Keiser 2010, 2012, 2014, 2015). While this is a plausible model, it puts extra constraints on the timing of the formation of the disc. This is estimated to take $\sim$0.1–10 Myr (see e.g. Shu et al. 1993; Vanhala & Cameron 1998; Tassis & Mouschovias 2004). This is on top of the time needed to form small bodies in the Solar system, which is $\sim$1–10 Myr (Hartmann 2005). If SLRs are injected during the molecular cloud stage, disc formation must occur quickly such that enough SLRs exist in the early Solar system.

In this paper, we investigate injection into an already formed disc as an alternative to this model. Injection would have to occur in the relativity early stages of the disc's lifetime, before small bodies begin to form. It is currently unknown at what point material can be injected and homogenized in order to be captured by forming meteorites. As all these processes are likely to occur simultaneously, simulations that track both injection and the subsequent formation into meteorites would go a long way to answering this question. However, this is beyond the scope of this paper.

The abundance of SLRs is typically parametrized by the ratios of ^{60}Fe and ^{26}Al to their stable isotopes. Quitté et al. (2005) and Tachibana et al. (2006) find a ^{60}Fe/^{56}Fe ratio of $\sim$(3–7) $\times 10^{-7}$. However, the technique used [secondary ion mass spectrometry (SIMS)] has been shown to give a significant positive bias (Ogliore, Huss & Nagashima 2011). Subsequent studies using a different technique (Tang & Dauphas 2012) show a lower ratio of 5×10^{-8}, although Mishra & Goswami (2014) use an improved SIMS method and find a ratio of 7×10^{-7}. Therefore, the true ratio is still unclear. However, if the lower estimates for the amount of ^{60}Fe are correct, then the ^{60}Fe/^{26}Al ratio becomes much lower than that generated by SNe (Gounelle & Meynet 2012). A possible resolution to this problem is suggested by Goodson et al. (2016), who note that different-sized dust grains are injected at different rates, and if they preferentially carry different SLRs, this could have a significant effect on the ^{60}Fe/^{26}Al ratio.

The amount of ^{60}Fe produced by an SN varies depending on the mass and metallicity of the exploding star. Calculations by Woosley & Weaver (1995) put the ^{60}Fe mass fraction at $\sim 2 \times 10^{-6}$ for a 20 $\mathrm{M}_{\odot}$ SN. Using initial Solar system abundances from Lodders (2003), Looney et al. (2006) calculate a meteoritic ^{60}Fe mass fraction of $1.10 \pm 0.38 \times 10^{-9}$.

We can define an enrichment fraction, f_{enr}, as the mass of SN material mixed into the disc as a fraction of the disc mass. Then, the change in mass fraction, X, of a given species, i, after enrichment can be calculated as

$$X_{i,\mathrm{after}} = (1 - f_{\mathrm{enr}})\, X_{i,\mathrm{before}} + f_{\mathrm{enr}} X_{i,\mathrm{supernova}}. \tag{1}$$

If the initial Solar system has no significant ^{60}Fe, then f_{enr} simply becomes

$$f_{\mathrm{enr}} = \frac{X_{i,\mathrm{after}}}{X_{i,\mathrm{supernova}}}. \tag{2}$$

Using $X_{i,\mathrm{after}} = 1.10 \times 10^{-9}$ and $X_{i,\mathrm{supernova}} = 2 \times 10^{-6}$ from above, this gives $f_{\mathrm{enr}} = 5.5 \times 10^{-4}$. Doing the same calculation for ^{26}Al ($X_{i,\mathrm{after}} = 3.77 \times 10^{-9}$ and $X_{i,\mathrm{supernova}} = 3 \times 10^{-6}$) gives $f_{\mathrm{enr}} = 1.3 \times 10^{-3}$.

The assumption of zero $X_{i,\mathrm{before}}$ is a contested one. It has been suggested (e.g. Gaidos et al. 2009; Young 2016) that successive SNe and massive stellar winds can allow a molecular cloud to self-enrich, such that stellar systems form with enriched material already embedded. This scenario is explored in simulations by Vasileiadis, Nordlund & Bizzarro (2013) and Kuffmeier et al. (2016). Using a turbulent periodic box, the evolution of a massive ($\sim 10^5\,\mathrm{M}_{\odot}$) star-forming region is followed over 20 Myr. It is found that SN feedback enriches the star-forming gas to a level that is largely consistent with that of the early Solar system, although the authors rely on numerical diffusion to mix the SN ejecta and cold gas. This model also remains somewhat controversial as it requires an age spread of star formation within the same cloud, which is at odds with observations (Elmegreen 2000; Jeffries et al. 2011; Soderblom et al. 2014) and simulations (Bonnell, Bate & Vine 2003; Dale, Ercolano & Bonnell 2012). While a non-zero value for $X_{i,\mathrm{before}}$ does not necessarily change the scenario investigated in this work, it would increase the mass fractions we see.

Variations in the SN mass can also produce quite large differences in the mass fraction, not to mention the inherent uncertainties in SN modelling. For example, Limongi & Chieffi (2006) calculate an ^{60}Fe mass fraction for a 20 $\mathrm{M}_{\odot}$ SN at 7.8×10^{-7}, 2.5 times less than that calculated by Woosley & Weaver (1995). Their ^{60}Fe mass fractions for the next nearest SN masses (17 and 25 $\mathrm{M}_{\odot}$) vary from the 20 $\mathrm{M}_{\odot}$ mass fraction by a factor of ∼1.5. With this in mind, f_{enr} is constrained only to a factor of 2 or 3 at best.

Hydrodynamical simulations of the interaction of an SNR with a circumstellar disc were performed by Ouellette, Desch & Hester (2007). They found that only a small fraction (∼1 per cent) of the disc mass is removed, in contrast to the ∼13 per cent expected from the analytical prediction of Chevalier (2000). They attribute this to the cushioning and deflecting effect of the bow shock in addition to the compression of the disc further into the gravitational well of the central star. However, their simulations are limited to two dimensions and face-on impacts. While an inclined disc might be expected to be disadvantageous for ablation, the geometry of the bowshock that shields the disc is likely to be substantially different and the impacting flow acts with the rotation of the disc on one side, reducing the threshold for ablation. This scenario therefore needs to be investigated. Ouellette et al. also found that only ∼1 per cent of the passing ejecta is captured by the disc. This is not enough to explain the observed abundances, although they suggest that dust grains might be a more efficient mechanism for injecting SLRs into the disc.

To investigate this possibility, Ouellette, Desch & Hester (2010) incorporated dust grains into their simulations. They found that about 70 per cent of dust grains larger than 0.4 μm are injected into the disc. This could potentially be enough to explain the observed abundances, although it relies on higher than observed dust condensation in the ejecta and the ejecta to be clumpy with the disc being hit by a high-density clump of ejecta. They estimate the probability of these conditions being met at 0.1–1 per cent and that the Solar system may be atypical in this respect.

The mixing effects of clumpy SN ejecta interacting with a molecular cloud were investigated by Pan et al. (2012). When the mixing is efficient, the enrichment fraction, defined as the ratio of ejecta mass to cloud mass, is $\sim 10^{-4}$. This is approximately the correct level, although as the SLRs are injected into the molecular cloud, and it takes of the order of a Myr to form stars and discs, the abundance of ^{60}Fe could be significantly reduced in this time.

The formation and subsequent evolution of a star–disc system under the effects of a supersonic wind were investigated by Li, Frank & Blackman (2014). They found that a disc can indeed form and survive in these conditions: A 10^{-3} $\mathrm{M}_{\odot}$ disc remains after being exposed to the wind for 0.7 Myr. However, their disc radius after formation is ∼1000 au, whereas discs near massive stars are typically photoevaporated down to tens of au (Johnstone et al. 1998). The flow speed is also much slower than that adopted by Ouellette et al. (2007), which, in turn, reduces the ram pressure significantly. Therefore, while their work was useful for investigating triggered star formation, the region of parameter space that they explored is unrealistic for disc ablation via nearby SN.

Recently, Goodson et al. (2016) performed three-dimensional (3D) simulations of the interaction of an SNR with a large (8.8 pc), clumpy molecular cloud, including dust grains. They found that the majority of large dust grains are injected into the molecular cloud, within 0.1 Myr of the SN explosion. They note that if ^{60}Fe and ^{26}Al preferentially condense on to different sized grains, this could explain the discrepancy in the ratio between the two SLRs.

This paper aims to improve and expand on the 2D hydrodynamical calculations of Ouellette et al. (2007) in a number of ways. First, by doing fully 3D simulations, more complex dynamics can be studied, and the angle between the disc and the flow can be varied. Secondly, we consider a range of disc masses (1 0.1 and 0.01 times their canonical disc mass), as disc density is the main factor in determining the extent to which a disc is ablated. By considering a number of disc masses spanning a range of mid-plane densities, we can investigate how different discs react and at what point the disc becomes significantly affected. Finally, we adopt time-dependent flow properties from a 1D simulation of the SNR. This provides more accurate flow conditions past the disc, compared to the analytical approximation used by Ouellette et al. (2007), particularly in the early stages of the SNR's expansion. We aim to better determine the nature of the interaction, the mass-stripping rate of the disc and the injection rate of SLRs into the disc.

2 MODELS

2.1 Overview

A stellar disc is simulated in three dimensions, with mass injected on to the grid to simulate the impact of an SNR. The strength of the flow is dependent on the size and distance of the SN and is time-dependent. To calculate this precisely, a simple, 1D simulation of a spherical SNR is performed. The evolution of the density, velocity and temperature is recorded at the desired distance from the SN, which can then be used by the main simulation to control the properties of the wind. This is in many ways simpler than performing an analytical approximation (e.g. Matzner & McKee 1999), and has the advantage of reproducing all the features of a realistic SNR, particularly in the early expansion.

2.2 The supernova remnant

The SN has an ejecta mass of 20 $\mathrm{M}_{\odot}$ and an ejecta energy of 10^{51} erg (following Ouellette et al. (2007) to represent a typical Type II SN), and is initially confined to a radius of 2000 au. The ambient medium is set to a density of 2.34×10^{-24} g cm^{-3} and a temperature of 10^4 K. The simulation parameters are noted in Table 1. For all simulations, the mean molecular weight $\mu = 2.4$ and $\gamma = 5/3$. The SN calculations were performed in spherical symmetry on a uniform 1D grid, extending to $r = 10^5$ au with 3200 cells. The same calculations were done at a half and s quarter resolution with identical results.

Fig. 1 shows how the fluid variables change over time at a point 0.3 pc from the origin of the SNR. 0.3 pc is chosen to aid comparison with Ouellette et al. (2007) and is consistent with observations of the Orion Trapezium Cluster. These values will determine the properties of the flow past the circumstellar disc in the 3D simulation. The SN

Table 1. SNR parameters.

Variable	Value
M_{ej}	20 $\mathrm{M}_{\odot}$
E_{ej}	10^{44} J
ρ_{amb}	2.34×10^{-24} g cm^{-3}
T_{amb}	10^4 K

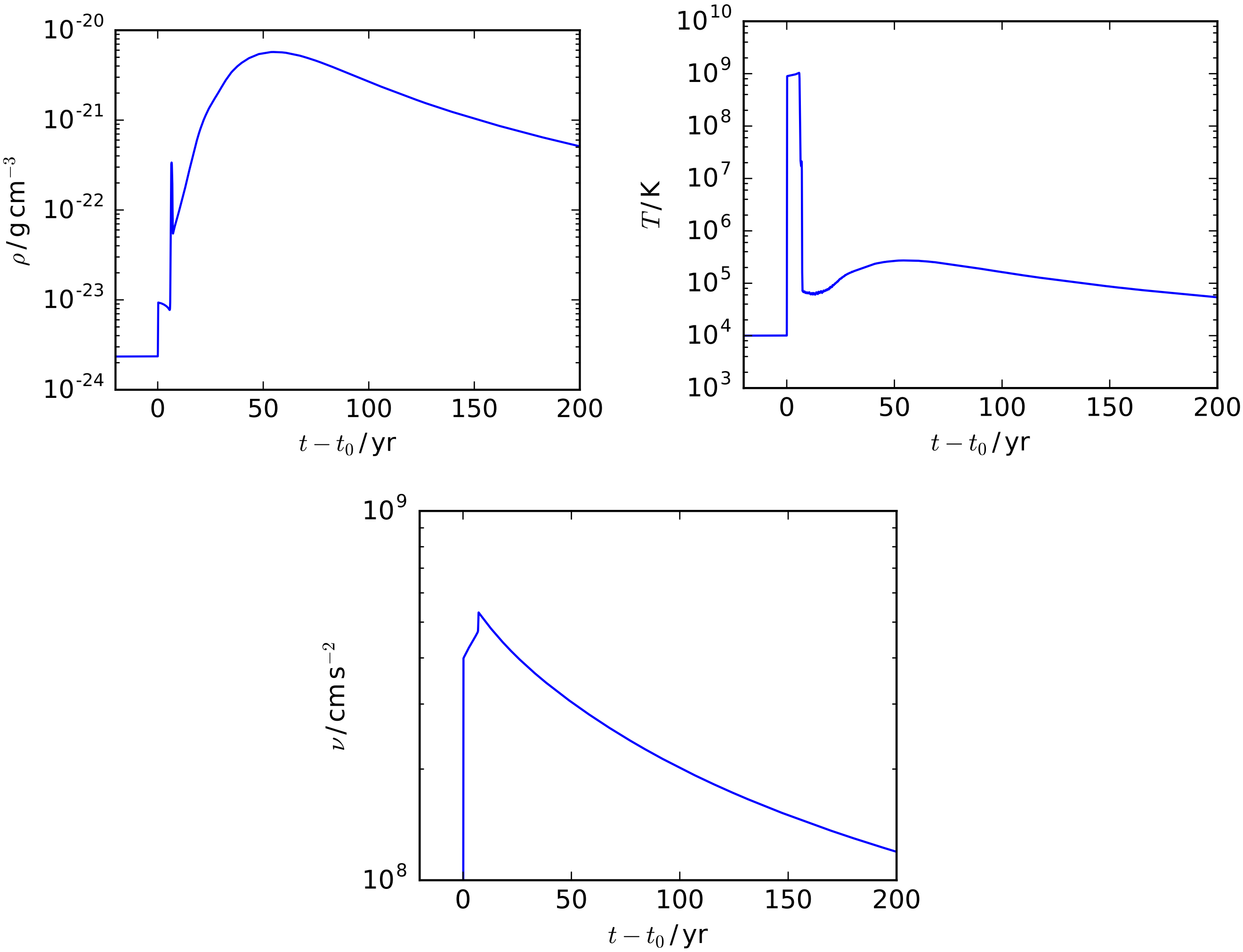

Figure 1. Density, temperature and velocity of the fluid 0.3 pc away from the SN as described in Section 2.2. t_0 is the time at which the SNR shockwave first reaches a radius of 0.3 pc ($t_0 \approx 55$ yr).

ejecta takes 55.4 yr to reach 0.3 pc, which is insignificant compared to the half-lives of the SLRs, so there is no significant decay during the travel time. The SNR is still in its free expansion stage at this point. The strength of the flow is parametrized by the ram pressure, $P_{\mathrm{ram}} = \rho v^2$, and is shown in Fig. 2. Also shown for comparison is the analytical ram pressure curve used by Ouellette et al. (2007), which is only a close approximation to the numerical results at late times. The interaction is strongest in the early stages, where the approximation is poor.

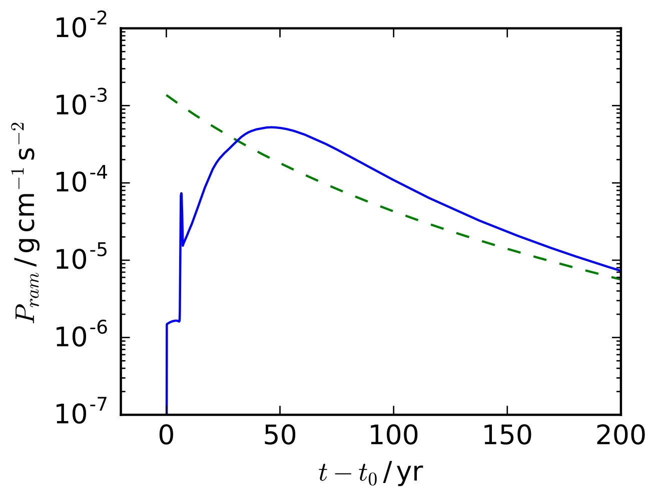

Figure 2. Ram pressure 0.3 pc away from the SN, as described in Section 2.2. t_0 is the time at which the SNR shockwave first reaches 0.3 pc. The dashed green line shows the ram pressure used by Ouellette et al. (2007) for comparison.

2.3 The circumstellar disc

The disc model is adapted from Gressel et al. (2013). The temperature is defined to be constant across z, and to be inversely proportional to cylindrical radius, R:

$$T(R) = T_0(R/R_0)^{-1}. \tag{3}$$

This gives the disc a constant opening angle. A constant opening angle is typically desirable as it allows the disc edge to align with cell boundaries in a spherical–polar domain. While this is not a concern for these simulations, it aids comparison with works in the literature. Defining the mid-plane density as

$$\rho_{\mathrm{mid}}(R) = \rho_0(R/R_0)^{-3/2}, \tag{4}$$

Table 2. Disc model parameters.

Variable	Value(s)
R_0	1 au
T_0	400 K
ρ_0	$\begin{cases} 3.5 \times 10^{-13}\ \mathrm{g\,cm^{-3}} \\ 3.5 \times 10^{-12}\ \mathrm{g\,cm^{-3}} \\ 3.5 \times 10^{-11}\ \mathrm{g\,cm^{-3}} \end{cases}$
$M_\star$	$1\,\mathrm{M_\odot}$

and enforcing hydrostatic equilibrium vertically, defines the 3D density structure, which can be derived as

$$\rho(\boldsymbol{r}) = \rho_{\mathrm{mid}} \exp\left(\frac{GM_*}{c_\mathrm{s}^2}\left[\frac{1}{r} - \frac{1}{R}\right]\right), \tag{5}$$

where c_s is the isothermal sound speed and r is the distance to the centre of the disc. Finally, the angular velocity, ω, is set to achieve radial equilibrium

$$\Omega(\boldsymbol{r}) = \Omega_\mathrm{k}(R)\sqrt{\frac{R}{r} - \frac{5}{2}\left(\frac{c_\mathrm{s}}{\Omega_\mathrm{k}(R)R}\right)^2}, \tag{6}$$

where $\Omega_\mathrm{k}(R) = \sqrt{GM_*}R^{-3/2}$ is the Keplerian angular velocity. The free disc parameters are chosen such that the disc resembles that described in Ouellette et al. (2005). As they observe no significant ablation of their disc, lower disc mass simulations are also performed, which are likely to be more susceptible to ablation. The values are summarized in Table 2. The disc is truncated at an inner radius of 4 au and an outer radius of 40 au. The temperature of the disc ranges from 100 to 10 K from the inner to outer disc boundaries. The outer rotation period is ~250 yr and the inner rotation period is ~10 yr. The initial ambient medium (ρ_{amb} and T_{amb}) is set to the same as that of the SN simulation for consistency (see Table 1). The disc was evolved in isolation and found to be stable for several outer rotation periods.

It should be noted that much bigger discs [with radii up to ~1000 au; see e.g. Bally et al. (2015)] have been observed. Such discs have a much larger surface area and the outer regions are less strongly held by the gravitational field, meaning that they will lose mass to ablation more readily. However, a 40 au disc is used here to aid comparison with previous work. Without good statistics of the disc radius at formation, it is also hard to say what is more typical, and in any case, it likely depends on unknown quantities such as the conditions under which the cluster formed. At larger radii, both the gravitational field strength and the disc's surface density decrease, making the material more tenuously held and more easily ablated. For a given disc model, only the central density and stellar mass determine the stripping radius: The stripping radius does not depend on the initial disc radius. With this in mind, some insight into the behaviour of larger discs can also be gleaned from our simulations.

3 THE SIMULATIONS

The calculations were performed with the hierarchical adaptive mesh refinement (AMR) code, MG (Falle 1991). The code uses the Godunov method, solving a Riemann problem at each cell interface, using piece-wise linear cell interpolation and MPI-parallelization. The Eulerian equations of hydrodynamics are solved using the second-order upwind scheme described in Falle (1991). Refinement is on a cell-by-cell basis and is controlled by error estimates based on the difference between solutions on different grids, i.e. the difference between the solutions on G_{n-1} and G_n determine refinement to G_{n+1}. Spatial resolution is doubled on each refinement level. Further details on the AMR method can be found in Falle (2005).

Table 3. Summary of the simulations. The disc angle (i) is defined as the difference in angle between the angular momentum vector of the disc and the vector of the flow direction, making 0° face-on and 90° edge-on. M_J is the mass of Jupiter.

Simulation	ρ_0/g cm^{-3}	$M_{\mathrm{disc}}/M_\mathrm{J}$	i (°)	Dynamic flow?
const00high	3.5×10^{-11}	8.22	0°	n
const00med	3.5×10^{-12}	0.822	0°	n
const00low	3.5×10^{-13}	0.0822	0°	n
const45low	3.5×10^{-13}	0.0822	45°	n
const90low	3.5×10^{-13}	0.0822	90°	n
dyn00low	3.5×10^{-13}	0.0822	0°	y
dyn45low	3.5×10^{-13}	0.0822	45°	y
dyn90low	3.5×10^{-13}	0.0822	90°	y

All simulations are performed on a 3D Cartesian grid, with the disc situated at the origin, and the plane of rotation aligned with the X–Y plane. For each simulation, a 'flow injection region' is defined where the values of the grid cells are set to the current SNR flow properties at the beginning of each time-step. This region is placed 96 au from the origin. The simulation region extends to ±256 au in all directions, except in the cases where this would create a large flow injection region. For all simulations, the lowest grid level has a resolution of 8 au, with four additional grid levels giving an effective resolution of 0.5 au. This gives 80 cells per disc radius. Detailed convergence studies for shock–cloud interactions (Pittard & Parkin 2016) indicate that a resolution of 32–64 cells per cloud radius is needed for signs of convergence, including in the mixing fraction. Although the scenarios are different, this provides some confidence that our simulations are of adequate resolution. They are also at a higher resolution than any previous studies of interactions of this type. A detailed resolution study is left to future work.

There are two reasons the disc is kept in the same orientation and the wind direction is changed (as opposed to vice versa). First, if the plane of rotation is not aligned to the direction of the grid, instabilities can develop and cause the disc to fragment with no outside influence (e.g. Davis 1984; Hahn, Teyssier & Carollo 2010; Hopkins 2015). Secondly, the grid is split among processors by dividing the domain along one of the grid directions. Placing the disc such that the divides split the disc across processors helps to distribute the computational load more evenly and allows the simulations to run more efficiently.

A set of eight simulations are performed. Table 3 details the differences between them. Some simulations are done with a constant flow, as this is the most straightforward to compare against analytical approximations. The parameters of the constant flow are defined by the peak ram pressure point of the SNR (see Figs 1 and 2) and occurs 55.8 yr after the disc is first hit by the SNR. The peak is taken as it represents the worst case scenario for the survival of the disc. Specifically, this is a density of 5.74×10^{-21} g cm^{-3}, a velocity of 2.87×10^8 cm s^{-1} and a temperature of 2.72×10^5 K. The corresponding ram pressure is 4.74×10^{-4} g cm^{-1} s^{-2}. In contrast, the flow in the dynamic simulations follows the temperature, density and velocity of the calculated SNR, shown in Fig. 1.

3.1 Defined quantities

In order to quantify the mass of the disc and the amount of SN ejecta that is captured by the disc, we define several quantities. The

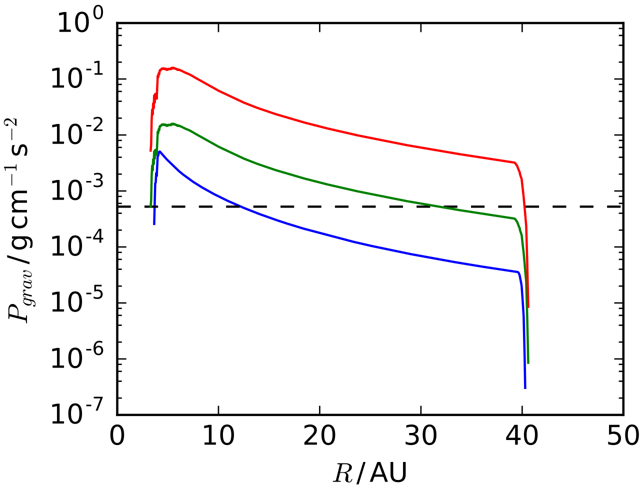

Figure 3. Gravitational pressure in the disc as a function of radius, as defined by equation (7). The blue, green and red lines correspond to the low, medium and high values of ρ_0 (see Table 3 for details). The dashed horizontal line shows the peak ram pressure of the SNR at 0.3 pc.

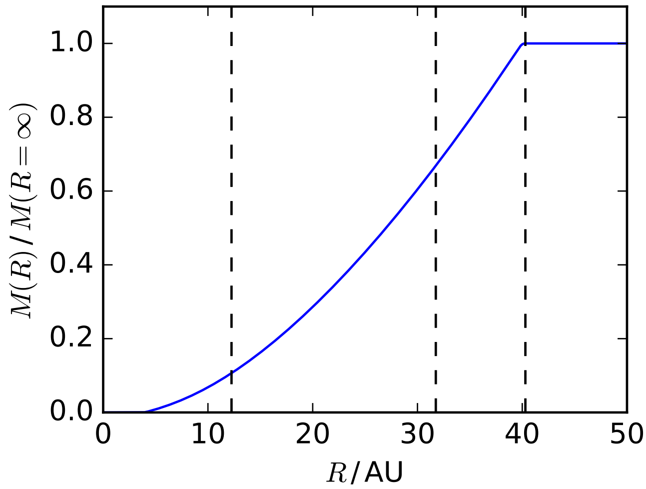

Figure 4. The fractional integrated mass of the disc as a function of disc radius. Note that this is the same for all values of ρ_0 for the density distribution given by equation (5). The dashed vertical lines show the radius outside which the gravitational pressure of the disc is less than the peak ram pressure of the SNR for each value of ρ_0. From the left- to right-hand side, the dashed lines are shown for low-, medium- and high-disc-mass cases.

mass of the disc, $M_{\rm disc}$, is defined as the total mass of gas that is bound to the central star's gravitational field, i.e. the velocity of gas in a given cell is less than the escape velocity at that point in space. The simulation uses an advected scalar to track the SLR-enriched SN ejecta. Disc material is given a scalar value of 0.0 and the enriched SN ejecta is given a scalar value of 1.0. Thus, for a given grid cell, the product of the advected scalar, the cell density and the cell volume gives the mass of enriched material in that cell. We define the mass of captured enriched material, $M_{\rm enr}$, as the total mass of enriched material that is gravitationally bound. Thus, the enrichment fraction $f_{\rm enr} = M_{\rm enr}/M_{\rm disc}$.

4 ANALYTICAL APPROXIMATIONS

Material in the disc will be disrupted if the ram pressure of the wind exceeds the gravitational force per unit area, $P_{\rm grav}$. This can be estimated as (Chevalier 2000)

$$P_{\rm grav} = \frac{GM_*\sigma}{R^2}, \tag{7}$$

where σ is the surface density of the disc. Fig. 3 shows the gravitational pressure as a function of radius for the three disc masses considered. By integrating surface density from the centre of the disc to the point at which the gravitational pressure drops below the peak ram pressure of the SNR, an estimate for the extent of the instantaneous stripping can be obtained.

Fig. 4 shows the cumulative integrated mass for the disc. If all the material at a gravitational pressure less than the peak ram pressure of the SN is stripped, then the low-mass disc is left with 10.7 per cent of its initial mass, the medium density disc retains 65.1 per cent and the high-mass disc retains 99.95 per cent.

In their investigation of the effects of inclination on the ablation of disc galaxies, Roediger & Brüggen (2006) provide an argument for why stripping should be independent of inclination angle for small angles. Assuming the gas disc to be infinitely thin, the force due to ram pressure on a surface element dA is $\rho_{\rm wind} v_{\rm wind}^2 \cos(i)$. The ram pressure is effectively reduced by a factor of $\cos(i)$. As the radial gravitational force is balanced with the centrifugal force only the force perpendicular to the plane of the disc contributes. This is also reduced by a factor of $\cos(i)$. This means that the criteria for material to be stripped from the disc are independent of the inclination angle. For highly inclined discs, the assumption of an infinitely thin disc will break down. While galactic discs are in a very different area of parameter space to stellar discs, these arguments are equally valid for either case.

5 RESULTS

Figs 5–7 show snapshots of the evolution of the disc with 2D slices though the 3D grid. Fig. 5 shows the evolution of discs of different masses subject to a constant flow. As expected, the more massive discs are more resilient to stripping. The low- and medium-mass discs are significantly deformed by the flow. For the low-mass disc, this breaks up the disc and forms a turbulent tail. However, in the medium-mass case, the deformed disc remains bound.

Figs 6 and 7 show the effect of inclination angle for the constant flow and dynamic flow cases, respectively. For inclined discs, the stripping is asymmetrical. For disc inclinations of 45°, the leading edge fragments and strips from the disc first, as the bow shock partially shields the trailing edge of the disc. As the disc continues to evolve, the trailing edge is stripped and the disc becomes more symmetrical again. As the 45° disc evolves, the disc is heavily stripped and eventually destroyed. At an inclination of 90°, the side of the disc rotating in the direction of the flow is stripped more heavily at first than the side rotating against the flow. Mass is stripped from the 90° disc much more slowly than for discs with lower inclinations, mainly due to the lower cross-sectional area of the disc to the flow.

The morphology of the constant wind and dynamic wind cases is broadly similar in all cases. The main distinguishing feature is that as the pressure of the dynamic wind starts to decrease, the tail becomes much wider.

The amount of mass bound to the star's gravitational well is shown as a function of time in Figs 8–10. Simulations with a constant flow exhibit an initial rapid ('instantaneous') stripping down to the level where the ram pressure is balanced by the gravitational pressure (where the disc mass plateaus), followed by a slower continual stripping caused primarily by the Kelvin–Helmholtz

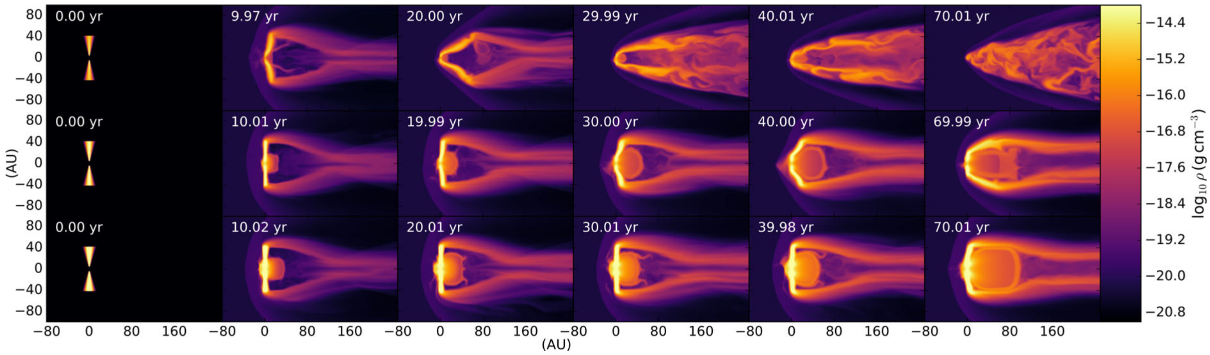

Figure 5. Slices through the *X*–*Z* plane at $Y = 0$ for the simulations of varying disc mass. The simulations from the top to bottom are const00low, const00med and const00high. The flow is constant and from the left- to right-hand side.

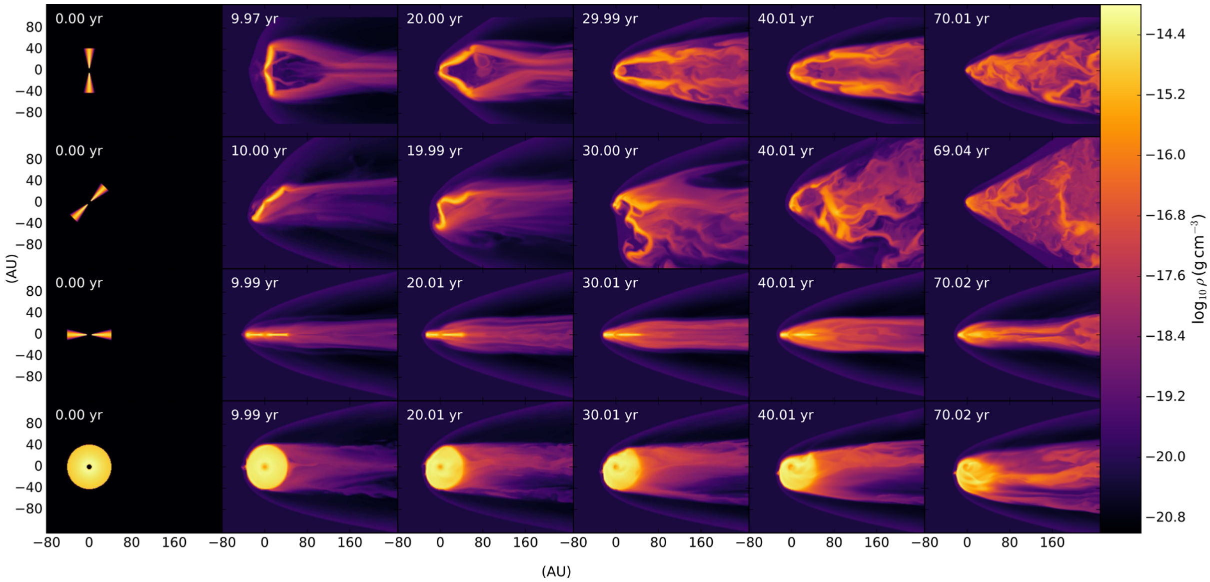

Figure 6. Slices through the *X*–*Z* plane at $Y = 0$ for the constant flow simulations. From the top to bottom: const00low, const45low and const90low. The bottom row also shows a slice though the *X*–*Y* plane at $Z = 0$ for const90low (the disc rotates clockwise in these images). Note that although the simulations are performed by changing the angle of the flow, the images here are rotated such that the flow in each image is from the left- to right-hand side in the plane of the slice. The asymmetry in the bottom row arises due to the rotation of the disc.

instability. Fig. 8 shows this for the three different disc masses simulated, together with the analytical approximations. For the low-mass disc, the analytical prediction fits the position of the plateau very well. The medium-mass disc begins to plateau but the continual stripping starts to dominate before it does so, pulling the mass below the analytical approximation. The high-mass disc loses virtually no mass due to instantaneous stripping and effectively starts in the continuous stripping phase. At the end of the simulation, both the medium- and high-mass discs are losing mass at a rate of $\sim 10^{-6}\,\mathrm{M_\odot\,yr^{-1}}$. During continuous stripping (between $t = 40$ and 70 yr), the mass-loss rate of the low-mass disc is $\sim 10^{-7}\,\mathrm{M_\odot\,yr^{-1}}$. While stripping is still occurring at the end of simulation, the constant ram pressure simulations are not continued beyond this point, as the longer the simulation runs, the more unrealistic the assumption of peak ram pressure is. Running the simulations for ≈150–250 yr provides enough data to establish trends and for comparison to other works.

As the inclination angle of the disc is increased, the stripping is generally slower (Figs 9 and 10). However, the difference between inclination angles of 0° and 45° is relatively small. Not only do they both plateau at about the same level, but they do so at about the same time (see Figs 9 and 10). This is because the flow in this instance is strong enough to deform the disc such that the initial inclination angle is no longer relevant. At high inclination angles, a different behaviour is observed, and the disc survives significantly longer at an inclination of 90°. The same general trend can be seen in Fig. 10 for the dynamic flow. Interestingly, for the face-on flow, the mass plateaus before the peak ram pressure has been reached, indicating that the history of the flow is important in shaping the disc and determining whether it is susceptible to ablation. The low-mass disc survives the dynamic flow only when placed edge-on to the flow, retaining nearly 60 per cent of its mass in this case (Fig. 10). The edge on disc is losing $\sim 2 \times 10^{-7}\,\mathrm{M_\odot\,yr^{-1}}$ at the end of the simulation. If this rate were to be sustained, the disc would be destroyed in ∼300 yr. However, the ram pressure decreases by two orders of magnitude in this time, so there will be some but not complete stripping during this period. The disc is therefore expected to survive significantly longer than we have simulated.

Fig. 11 shows the *z*-direction mass flux of the disc material at the end of simulation const00high. To show the regions where the disc is losing mass, the unbound material is shown in the right-hand panel. Mass is lost from two main regions: along the sides of the

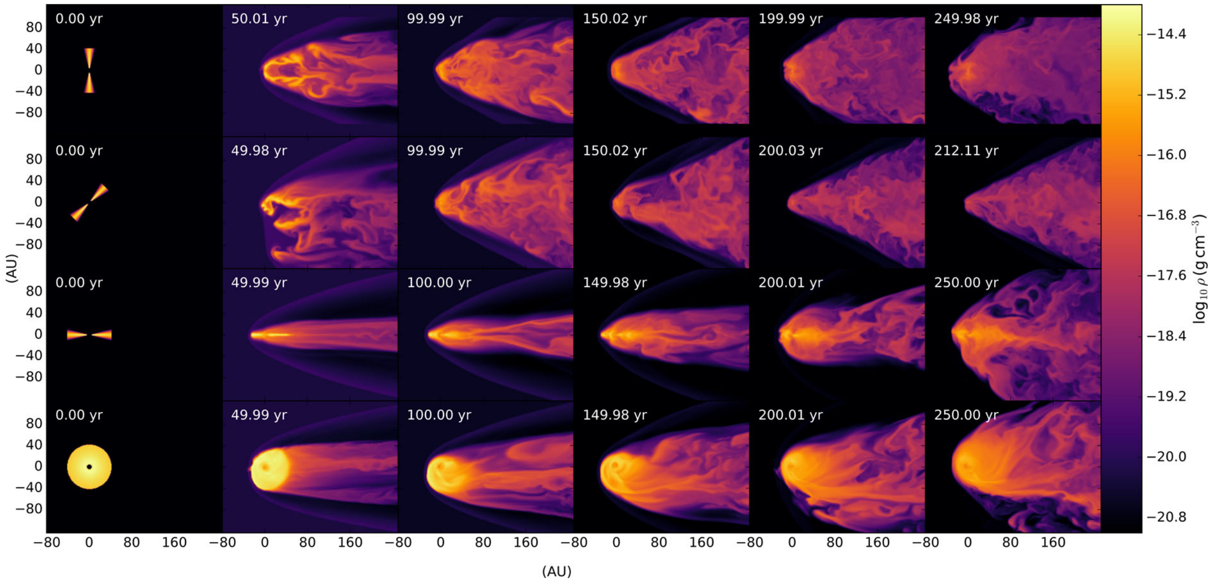

Figure 7. Same as Fig. 6 but for the dynamical flow simulations: dyn00low, dyn45low and dyn90low.

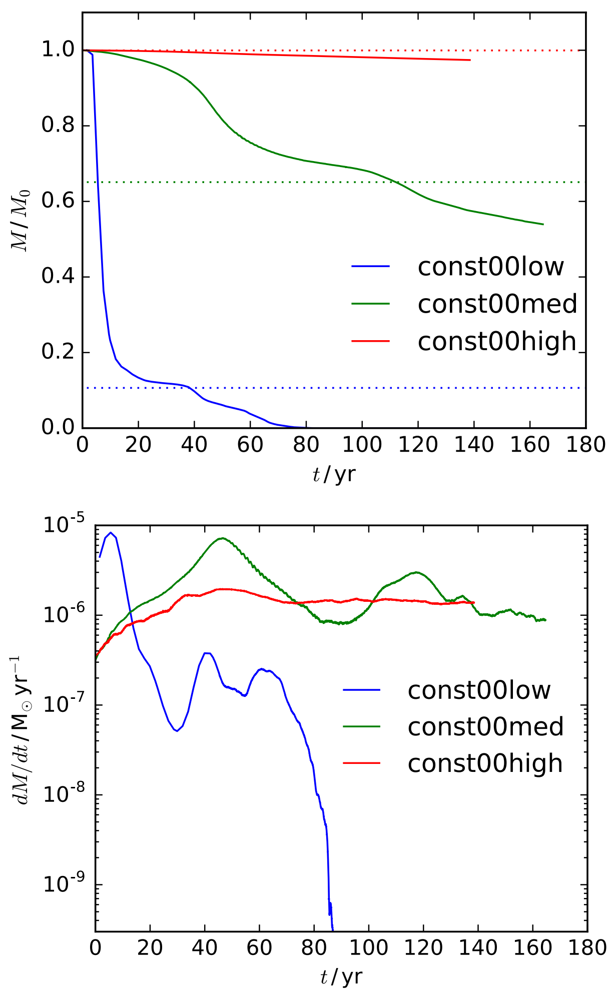

Figure 8. The upper panel shows the mass of the disc as a function of time for constant face-on flows, showing the three different disc masses simulated. The dashed lines show the corresponding analytical predictions from Section 4. The lower panel shows the mass-loss rates for the same three simulations.

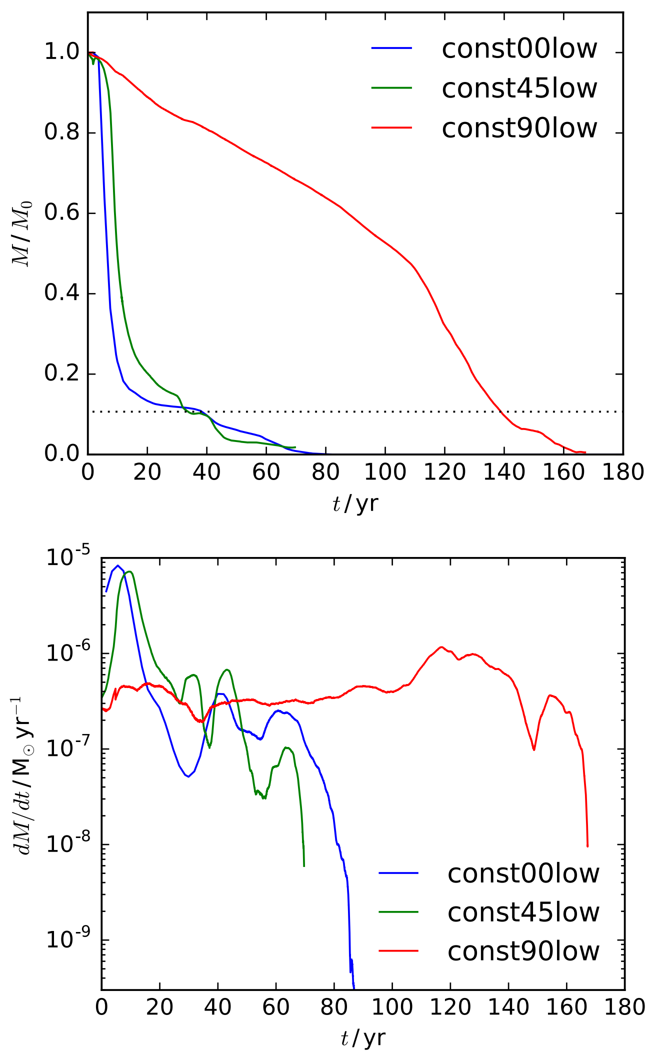

Figure 9. Same as Fig. 8 but for the different inclinations of the low-mass disc in a constant flow. The black dotted line shows the analytical predictions from Section 4.

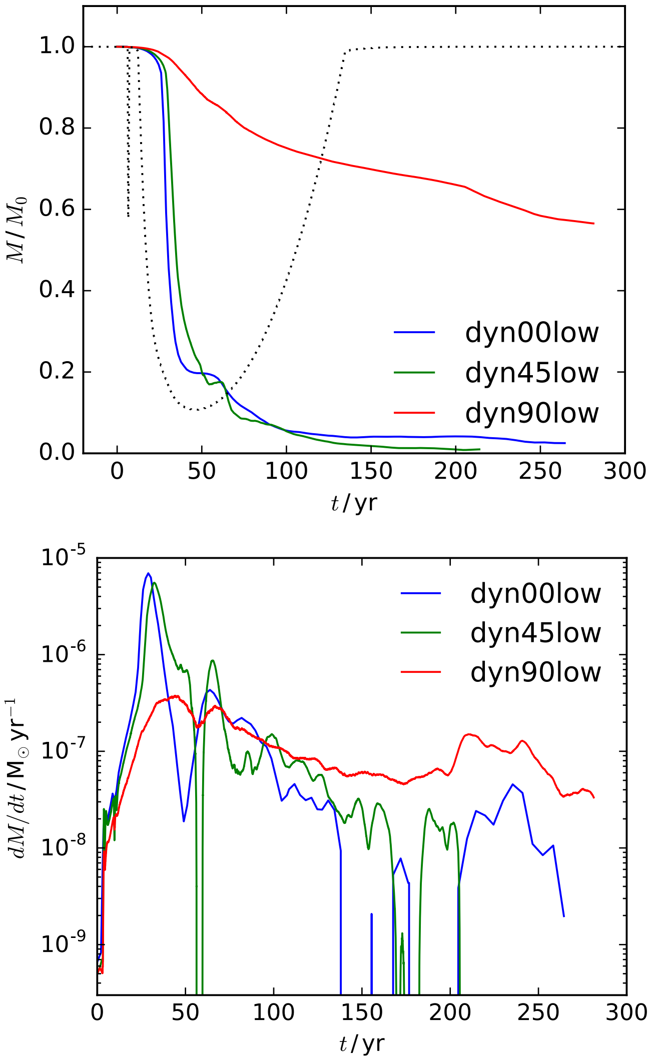

Figure 10. As Fig. 9 but for a dynamic SN flow. The dashed black line represents the fraction of the initial disc mass that is vulnerable to stripping as the ram pressure evolves.

deformed disc and also though the central hole. While the mass flux in both these areas is similar, the central region spans a much smaller area. Fig. 12 shows the same mass flux as Fig. 11, now multiplied by a factor of $2\pi r$ to account for the differing contributions to the total mass flux. It is clear that the majority of the mass is lost from the edge of the disc. Ablation from the centre of the disc accounts for approximately 30 per cent of the mass being ablated at this point in the disc's evolution.

Fig. 13 shows the amount of SN ejecta that becomes bound to the disc, tracked using an advected scalar. The discs in simulations const00med, const00high and dyn90low are the only discs to survive to the end of simulation and the only ones that could be considered to be enriched by SN ejecta, although all simulations are shown for completeness. The mass of SN ejecta in the disc is $\sim 10^{-9}$ M$_\odot$ for the two face-on discs and $\sim 10^{-10}$ M$_\odot$ for the edge-on disc.

Figs 14–16 show the distribution of bound material for the three discs that survive until the end of the simulation. The right-hand panels in these figures show the value of the advected scalar used to trace SN ejecta: A value of 1.0 indicates pure ejecta and a value of 0.0 indicates that no SN ejecta is present. In all three figures, the bound SN ejecta is predominantly found on the upstream face (or edge) of the disc. For the edge-on disc, the SN ejecta that becomes bound

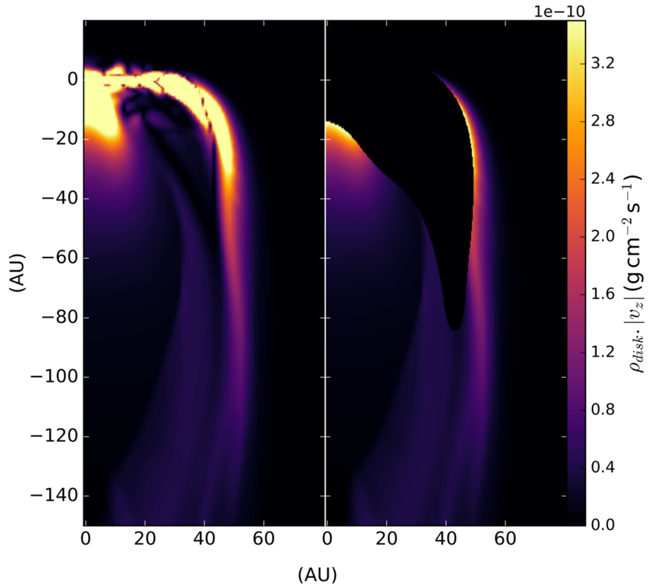

Figure 11. Absolute value of the mass flux in the X–Z plane for const00high at t = 140 yr. The left-hand plane shows the total contribution to the mass flux from the disc material. The right-hand plane shows only disc material that is gravitationally unbound from the central star.

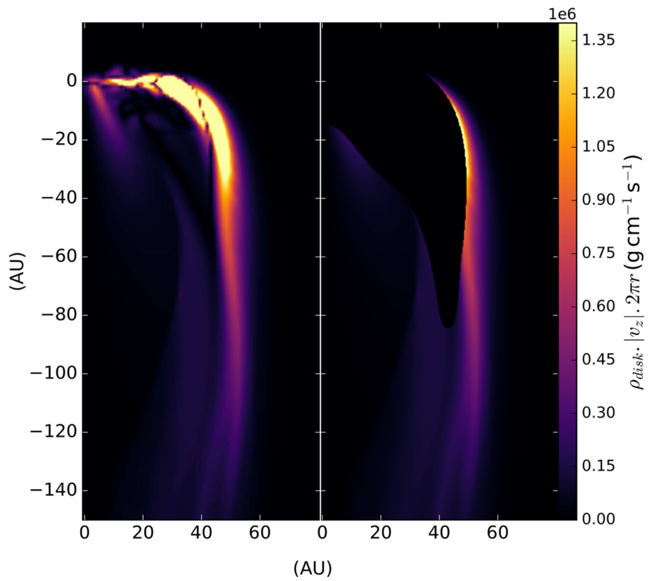

Figure 12. Same as Fig. 11, but showing the mass flux multiplied by a factor of $2\pi r$.

enters an orbit around the edge of the disc. The ejecta concentration on the leading surface is of the order of one part in 10^4 (in some small localized low-density regions, the concentration is at the 1 per cent level). Inside the disc, the concentration drops to typically one part in 10^5–10^6. Thus, we see some ejecta material being deposited on to the surface of the disc, but little mixing into the disc interior on the time-scales of our simulations. While our simulations do not run long enough to capture the subsequent mixing of this material (nor are turbulent motions within the disc properly resolved), Boss (2013) provide good estimates of the time-scales over which mixing is likely to happen, finding that homogenization in a 40 au disc occurs on time-scales of 10^3–10^4 yr. No significant decay of SLRs would be expected over this time frame.

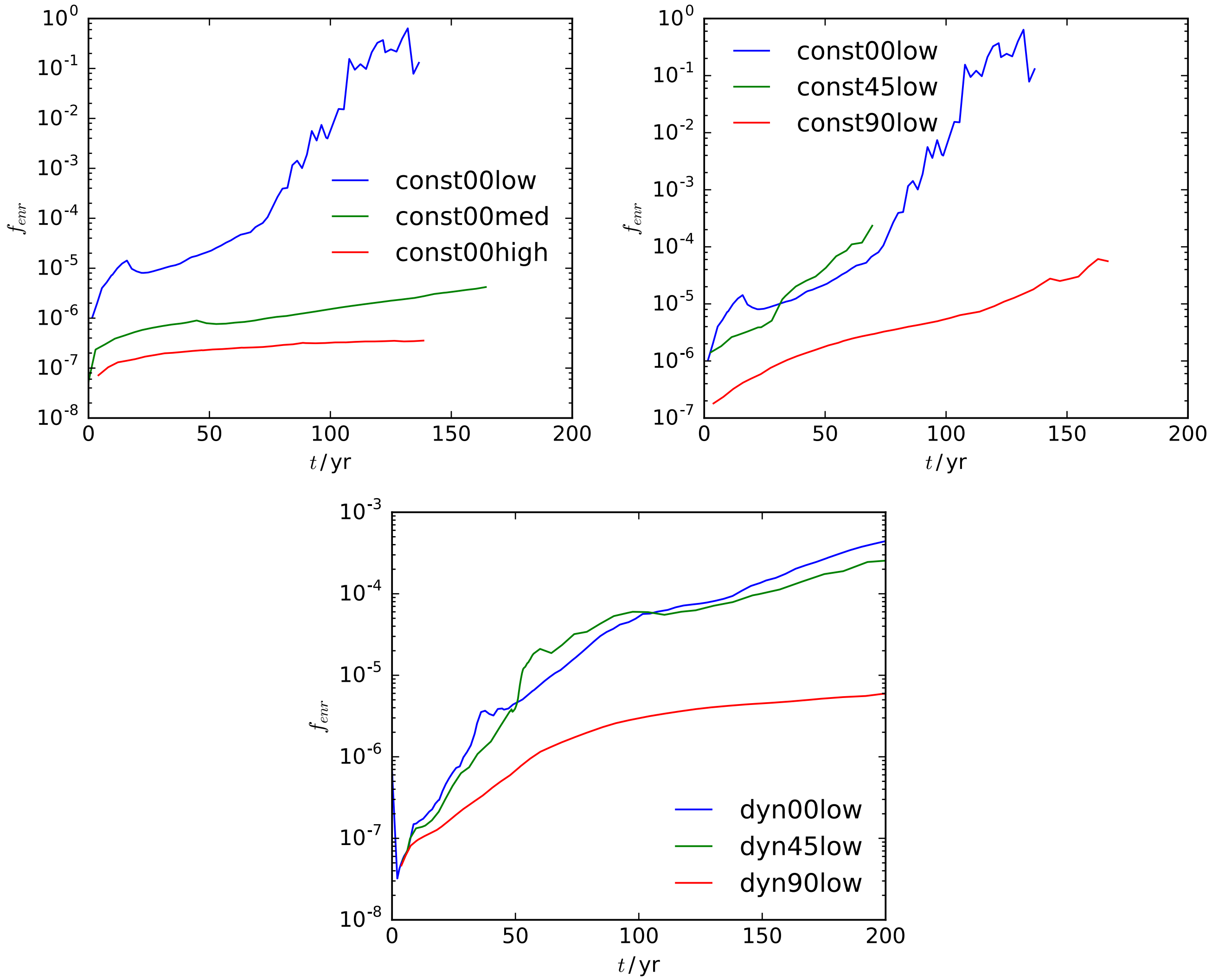

Figure 13. Enrichment fraction ($f_{\rm enr}$; see Section 3.1) as a function of time. The only discs to survive until the end of simulation are const00high, const00med and dyn90low. The relatively high enrichment fractions of the other discs (particularity const00low) at late times can be attributed to a dramatic reduction in $M_{\rm disc}$.

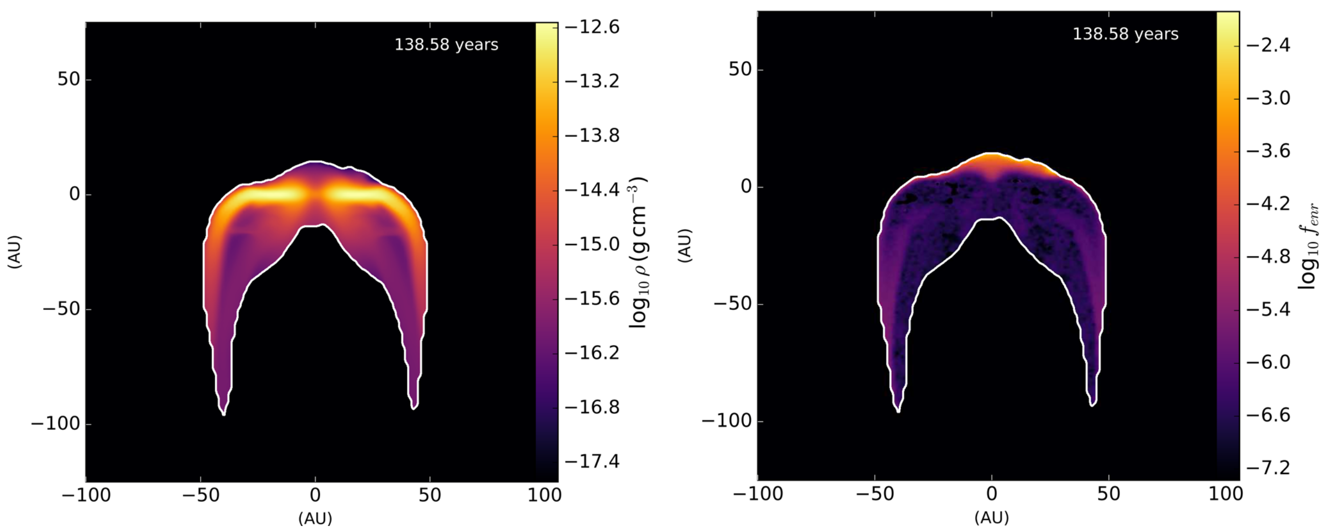

Figure 14. A slice though the *X*–*Z* plane at the end of simulation const00high, showing only material bound to the central star's gravitational potential. The left-hand image shows the total mass density. The right-hand image shows the value of the advected scalar used to trace SN ejecta material. It is equivalent to the enrichment fraction on a per cell basis (see 3.1). The edge of the bound region is highlighted in white to aid comparison between the two images.

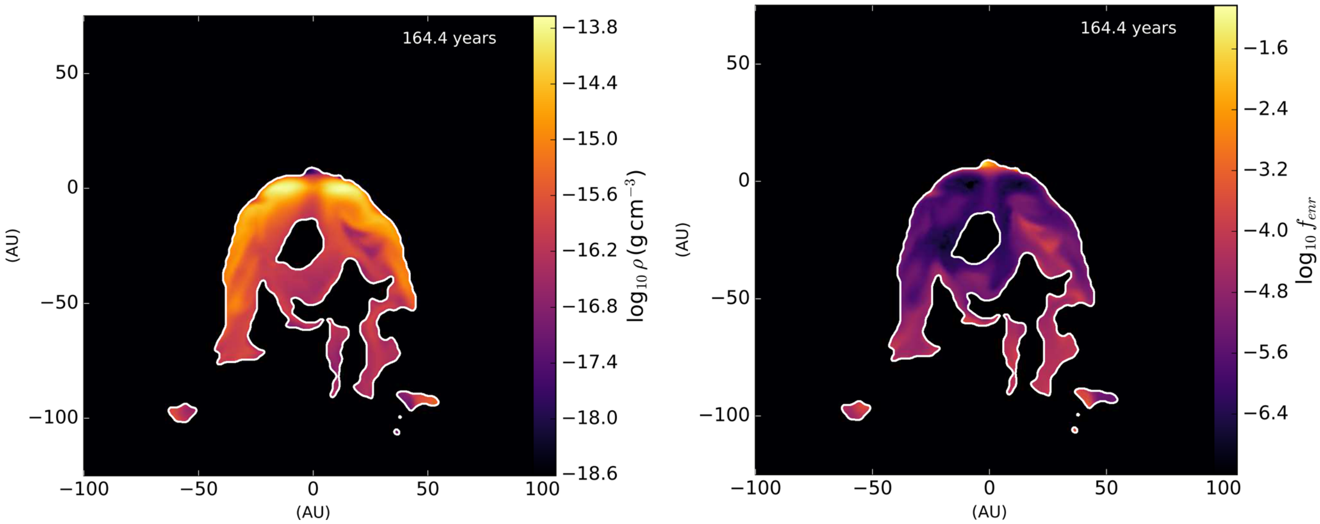

Figure 15. Same as Fig. 14 but for const00med.

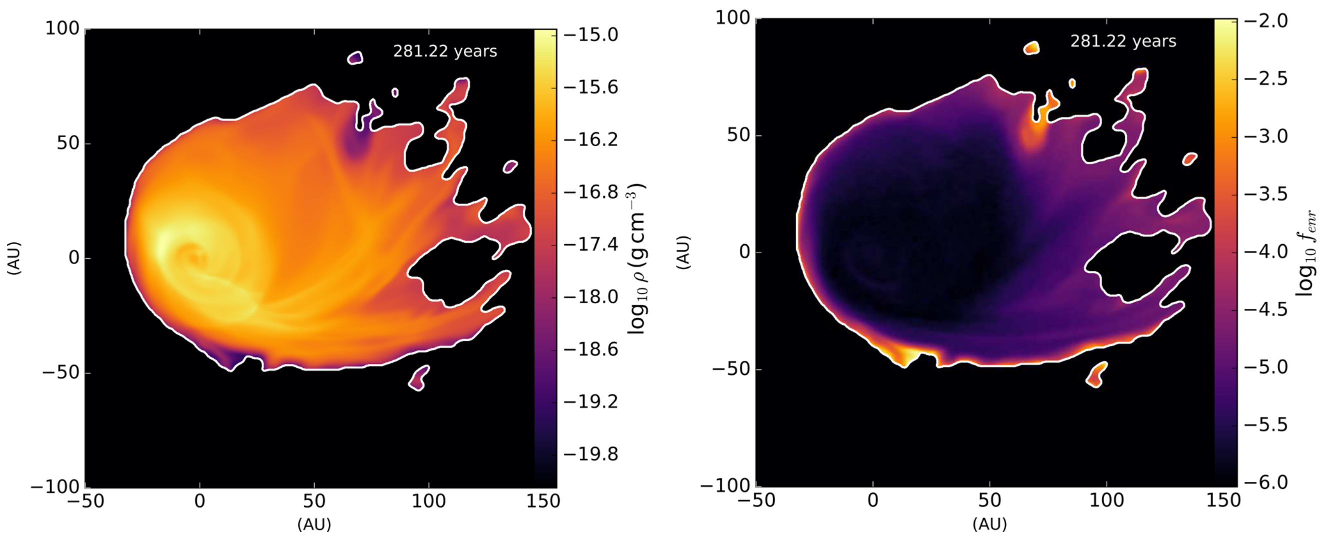

Figure 16. Same as Fig. 14 but for dyn90low, and showing slices though the *X*–*Y* plane.

6 DISCUSSION

6.1 Comparison to previous works

The main point of comparison is with Ouellette et al. (2005). Our face-on high-density disc can be considered equivalent to their canonical disc. Good agreement is obtained in that virtually no stripping is seen in either case. However, they see less than 0.1 per cent mass lost over 2000 yr, whereas we see ∼2.5 per cent lost over 140 yr. This difference can be attributed to the fact that our high-density disc is simulated only for the constant ram pressure flow where the long-term ablation is much stronger, whereas Ouellette et al. (2005) used a time-varying flow. Our simulations also differ in that we observe consistency with the analytical predictions of Chevalier (2000), whereas they state that the bow shock shields the disc, causing it to be able to survive higher levels of ram pressure.

Li et al. (2014) study the effect of triggered star formation, allowing a disc to form and evolve under the effects of a wind. Their simulations are in a very different region of parameter space from ours: The ram pressure of their wind is approximately seven orders of magnitude lower, so they are observing the interaction on a time-scale of Myr, and their disc after formation has a radius of ∼1000 au, with a resolution of 23 au. However, they do note that at the end of their simulation, the disc radius is much less than that predicted using the method of Chevalier (2000).

As there have been no studies specifically of the ablation of inclined stellar discs, the only comparison that can be made is with galactic discs. Roediger & Brüggen (2006) and Jáchym et al. (2009) both specifically investigated the effect of inclination on the ram pressure stripping of galactic discs. We observe the same general dependence on inclination angle, where stripping is similar for low inclination angles and is only strongly impeded for close to edge-on orientations. We also observe the same asymmetry when discs are not face-on. Jáchym et al. (2009) argue that the parallel side is stripped more easily as the wind works in the direction of rotation to push the material off the disc, whereas the material on the antiparallel side must first be slowed to zero velocity and re-accelerated in the opposite direction if it is to be stripped on that side on the disc (otherwise it will continue to orbit round to the other side of the galaxy where it may then be stripped more easily). Roediger & Brüggen (2006) note that after an outer rotation period, the disc becomes symmetrical again, as the entire disc has experienced the side with stronger stripping.

For galactic discs, the stripping occurs over a relatively long period of time, with the disc experiencing several rotation periods while being ablated. However, the nature of the stripping depends on how the galaxy is orbiting within the cluster. A galaxy on a circular orbit will experience constant ram pressure throughout its lifetime, whereas a galaxy falling radially will experience a shorter peak of ram pressure. Roediger & Brüggen (2007) calculate the dynamic ram pressure for several different orbital paths a galaxy might take. Defining a significant ram pressure as one that would be expected to strip at least half of the disc mass if maintained constantly (this corresponds to what Roediger & Brüggen 2007 refer to as a 'medium' ram pressure and is $\sim10^{-11}\,\mathrm{g\,cm^{-1}\,s^{-2}}$ in their case), the galactic disc experiences significant ram pressure for ∼0.75–2 times the outer rotation period during each orbit.

For the SN and stellar disc interaction examined here, the ram pressure is significant for only approximately one-third of the outer rotation period. This means that it is possible for the stellar disc to maintain asymmetry after the point where stripping is significant, although it is not clear where the boundary lies, either in terms of ram pressure or rotation periods, in order for this to occur. Also note that this effect requires the flow to impact the disc edge-on or near edge-on for extended periods, whereas a galaxy is likely to experience stripping from a number of different angles at different points in its orbit.

6.2 Internal stripping

Our simulations show that a significant amount of mass is lost though the central hole of the disc during the continuous stripping phase. Theoretical considerations show that large planets can cause gaps to form in the disc (Takeuchi, Miyama & Lin 1996), and observations of protoplanetary discs have since detected the presence of such gaps (Calvet et al. 2002; Andrews et al. 2016). If these gaps are large and deep enough, they could provide additional channels for ablation to take place.

Similarly, in disc galaxy simulations, cooling causes the disc to fragment and allows the wind to flow though areas of low density within the galaxy (Tonnesen & Bryan 2009). This causes the instantaneous stripping to proceed faster but to the same radial extent compared to the adiabatic, non-fragmented disc. The differences in long-term stripping were not investigated but it is likely to be accelerated in the same way by the additional surface area, and will almost certainly affect the morphology of the flow. However, cooling is not significant in the bowshock surrounding the disc in our simulations. This may change if the SNR shock itself became strongly cooling (due to a greater age at the time of interaction, and/or higher circumestellar densities).

6.3 Continuous stripping

A number of different authors (Nulsen 1982; Hartquist et al. 1986; Arthur & Lizano 1997) have provided estimates for the mass-loss rate of a pressure-supported globule under the effect of a wind. All their estimates are based on the mass-loss rate of the globule being, due to conservation of momentum, approximately equal to the mass flow rate though the cross-sectional area of the object being ablated, i.e. $\dot{M} = \pi r^2 \rho_{\rm wind} v_{\rm wind}$. Calculating this value for the constant wind used for our simulations gives $\dot{M} = 3\times10^{-8}\,\mathrm{M_\odot\,yr^{-1}}$, which is around 100 times lower than the value seen in the simulations ($\sim10^{-6}\,\mathrm{M_\odot\,yr^{-1}}$). The flaw in this argument when applied to discs is that each parcel of gas already contains a large amount of momentum due to its rotation. For protoplanetary discs, the pressure support is relatively weak so the velocity of the gas is close to Keplerian and thus the escape velocity. This means that the incoming wind needs to transfer a smaller proportion of its momentum to the gas in the disc so that it becomes unbound. In practice, this interaction is fairly complex, particularly for non-face-on orientations, and there have been no simple analytical formulae proposed, but it is clear that it is not well described by those for simpler, non-rotating objects.

Photoevaporation by a nearby massive star can also play a role in disc dispersal, and is thought to be the cause of the proplyd objects in the Orion Nebula (Henney & Arthur 1997). Störzer & Hollenbach (1999) model the effect of an external source of ultraviolet radiation on circumstellar discs, finding good agreement with their models and observations of the Orion proplyds. They provide a crude fit to their results for the mass-loss rate:

$$\dot{M} \approx 10^{-7}\,\mathrm{M_\odot\,yr^{-1}}\left(\frac{r_{\rm disc}}{100\,\mathrm{au}}\right)^{1-1.5}, \tag{8}$$

at a distance of 0.2pc from a θ^1 Ori C-like star. Richling & Yorke (2000) perform a similar analysis and find agreement with the above equation. Calculating this value for a disc of $r_{\rm disc} = 40\,\mathrm{au}$ gives $\dot{M} = 3\times10^{-8}\,\mathrm{M_\odot\,yr^{-1}}$. This is ∼100 less than the continuous stripping rate from the SNR interaction at a distance of 0.3 pc for models const00med and const00high. The lifetime of the const00med and const00high discs to photoevaporation, $t_{\rm life} \approx M_{\rm disc}/\dot{M}$, is thus 3×10^4 and 3×10^5 yr, respectively. This indicates that photoevaporation can be an important process that may destroy discs before any nearby massive star explodes as an SN. However, not all discs will be exposed to as high a UV flux as that occurs in Orion, despite still being subject to the effects of a nearby SN explosion (for instance, a B0V star has an ionizing flux that is 1.5 times lower than θ^1 Ori C). In addition, more massive discs than we have considered may survive photoevaporation from Orion-like UV fluxes for several millions of years before being subject to an SN explosion.

Another possible source of ablation for stellar discs is the wind from a nearby massive star. This can last much longer than the SNR. For massive stars ($M \gtrsim 25\,\mathrm{M_\odot}$), the strongest wind occurs during the Wolf–Rayet (WR) phase, which lasts ∼0.3 Myr. For an isotropic wind, the ram pressure at a distance r is

$$P_{\rm ram} = \frac{\dot{M}}{4\pi r^2 v}, \tag{9}$$

where $\dot{M}$ is the mass-loss rate of the star and v is the velocity of the stellar wind. Typical values for the star's wind during the WR phase are $\dot{M} = 10^{-5}\,\mathrm{M_\odot\,yr^{-1}}$ and $2\times10^{-8}\,\mathrm{cm\,s^{-1}}$, giving a ram pressure of $1.2\times10^{-8}\,\mathrm{g\,cm^{-1}\,s^{-2}}$. This is several orders of magnitude lower than what appears in any of the three disc masses simulated (see Fig. 3), so no direct stripping is possible. While there may be some long-term, continuous stripping, we expect stripping from photoevaporation to dominate such periods.

In conclusion, photoevaporation and hydrodynamic ablation are processes that can both affect the disc prior to it being subject to an SN explosion. However, we expect some discs to survive these earlier processes. For those that do, SN-induced stripping can far exceed the photoevaporative mass-loss rate and clearly dominates the mass-loss rate during the interaction of the disc with the SNR. This is the scenario that we study in this work.

A final issue concerns the fact that the radiation and winds of nearby massive stars will alter the ambient medium into which the SN explodes. For instance, a steady wind will produce a density profile that declines as r^{-2}. Alternatively, the massive star may undergo an outburst and eject a dense shell of gas (perhaps the most famous example of this is the Homunculus Nebula produced by η Carinae). However, unless the mass that the SNR encounters is comparable to the ejecta mass, the SNR will remain in its free-expansion phase and thus, its dynamics will be largely unaffected by the surrounding material. In our simulations, the swept-up material is a tiny fraction of the ejecta mass at 0.3 pc (∼0.015 per cent for the SNR values used here).

6.4 Planet formation

As planet formation occurs on time-scales much longer than the SNR interaction simulated in this work, the disc is likely to re-establish equilibrium before planets begin to form. As far as planet formation is concerned, the interaction is therefore equivalent to replacing the disc with one of smaller mass.

6.5 Enrichment via SN

Overall, very little mass from the SNR flow becomes bound to the disc: $\sim10^{-9}$ M$_\odot$ for face-on discs that survive the stripping (models const00med and const00high) and $\sim10^{-10}$ M$_\odot$ for the edge-on disc that survives (model dyn90low). This is about 10 times less than seen by Ouellette et al. (2007). Some of the difference may be due to the differences in the dimensionality of the simulations (3D in our case, 2D in theirs). However, most of it is likely due to differences in the radiative cooling (which is included in their simulations, while ours are adiabatic). Thus, the hot SN ejecta is more able to cool down and mix with the disc in their simulations. The broad conclusion is the same, however, that the enrichment of protoplanetary discs via SN ejecta by pure hydrodynamic mixing is too inefficient to explain the abundance of SLRs in the early Solar system. The highest value of $f_{\rm enr}$ seen in our simulations with surviving discs is $\approx5\times10^{-6}$ (in model dyn90low – see Fig. 13), which falls short of the 10^{-4} needed using SLR production values from Woosley & Weaver (1995). Interestingly, this is for our low-mass, edge-on case. Low-mass discs obviously benefit more from the same amount of ejecta material, but are also generally destroyed more easily. However, we believe that the fact that edge-on discs survive significantly longer than face-on discs allows such discs to intercept more of the SN ejecta, and thus have the highest enrichment fraction. So, at least for the particular parameters chosen here, a low-mass edge-on disc can be enriched more than a high-mass face-on disc. While the discs here do not meet the enrichment requirements deduced from observations, it may be possible that a much larger disc (and hence larger surface area for collection) placed further away from the SN (such that its outer parts do not get instantaneously stripped) could be more efficient at absorbing SN ejecta. This is left for the subject of future investigation.

We have also considered only gas phase ejecta. It has been suggested (by e.g. Goodson et al. 2016) that dust grains would be able to penetrate and be absorbed more easily into the disc. However, the abundance of dust grains in the SNR is uncertain (see e.g. Bianchi & Schneider 2007; De Looze et al. 2017). The dust must also survive the reverse shock as the SNR interacts with the surrounding medium (Micelotta, Dwek & Slavin 2016), although this may not be significant for the close-proximity SNRs required for disc enrichment.

Finally, we note that the enrichment that we see in our simulations is limited to the surface of the disc. The time-scales in our simulations are too short for mixing of the SLRs throughout the disc (Boss 2013, note a mixing time of 10^4 yr), and in any case, the resolution is such that we do not adequately resolve the motions responsible for mixing material within the disc.

7 CONCLUSION

We have presented 3D simulations of the stripping of stellar discs due to the influence of a nearby SNR, using a physically motivated dynamic flow. We have also investigated the effect of varying the inclination angle and disc mass. While a number of other processes (e.g. photoevaporation and ablation by the radiation field and wind from a nearby massive star) can cause significant stripping, or even complete destruction of the disc, prior to interaction with an SNR, this is not always the case. We therefore assume in our investigation that at least some part of the disc is present when a nearby massive star explodes.

Good agreement is found with the analytical predications of Chevalier (2000). However, this accounts for only part of the stripping as Kelvin–Helmholtz instabilities can cause additional material to be ablated. In the initial, instantaneous stripping phase, a flow at the peak ram pressure can strip 90 per cent of a low-mass disc ($M_{\rm d}\sim0.1M_{\rm J}$) and 30 per cent of a medium-mass disc ($M_{\rm d}\sim1.0M_{\rm J}$) on time-scales of 10–100 yr (less than one outer rotation period). High-mass discs ($M_{\rm d}\sim10M_{\rm J}$) are largely unaffected by instantaneous stripping.

During continuous, longer term, ablation, discs lose mass at a rate of $\sim10^{-6}$ M$_\odot$ yr^{-1}. This value decreases with time as the SNR passes and the flow weakens, but is several orders of magnitude greater than the mass-loss rate due to photoevaporation or stellar wind ablation and will therefore dominate the disc's mass-loss rate during this time.

We find that the inclination angle only has a large effect on the evolution when the disc is close to edge-on (similarly to previous findings from simulations of disc galaxies). When the ram pressure is large compared to the gravitational pressure in the disc, low-inclination-angle discs are deformed to the point that their evolution converges to that of a face-on (0° inclination) disc. In contrast, our edge-on discs show a much steadier rate of mass-loss (instantaneous stripping is much reduced due to the lower cross-section) and can survive significantly longer than their face-on counterparts. Amongst the low-mass discs simulated, only the edge-on disc survived interaction with the SNR (retaining almost 60 per cent of its mass).

The stripping of inclined discs can be quite asymmetrical, and the direction of the stripped tail may not line up with the direction of the flow (also like disc galaxies). However, unlike disc galaxies, the flow may die down before the asymmetries have disappeared. For the SNR parameters chosen, the interaction is very short, lasting only a couple of hundred years. This means that stellar discs are unlikely to be observed during this period, but seeing an asymmetric disc may be evidence that it underwent this type of ablation in its past. For discs more distant from the SN, the duration of significant interaction will be longer.

Amongst all of our simulations, the highest ejecta enrichment fraction is 5×10^{-6}, which is too low to explain the presence of SLRs in the early Solar system. The highest enrichment is seen in a low-mass edge-on disc, suggesting that the ideal case for enrichment is a low-mass edge-on disc (which would be destroyed if placed face-on) rather than a face-on disc that one might naively assume.

ACKNOWLEDGEMENTS

The calculations for this paper were performed on the DiRAC 1 Facility jointly funded by STFC, the Large Facilities Capital Fund of BIS and the University of Leeds.

REFERENCES

Anderson K. R., Adams F. C., Calvet N., 2013, ApJ, 774, 9
Andrews S. M. et al., 2016, ApJ, 820, L40
Arthur S. J., Lizano S., 1997, ApJ, 484, 810
Bally J., Sutherland R. S., Devine D., Johnstone D., 1998, AJ, 116, 293
Bally J. et al., 2015, ApJ, 808, 69
Balog Z., Rieke G. H., Su K. Y. L., Muzerolle J., Young E. T., 2006, ApJ, 650, L83
Bertoldi F., Jenkins E. B., 1992, ApJ, 388, 495
Bianchi S., Schneider R., 2007, MNRAS, 378, 973
Bonnell I. A., Bate M. R., Vine S. G., 2003, MNRAS, 343, 413
Boss A. P., 2013, ApJ, 773, 5
Boss A. P., Keiser S. A., 2010, ApJ, 717, L1
Boss A. P., Keiser S. A., 2012, ApJ, 756, L9
Boss A. P., Keiser S. A., 2014, ApJ, 788, 20
Boss A. P., Keiser S. A., 2015, ApJ, 809, 103
Calvet N., D'Alessio P., Hartmann L., Wilner D., Walsh A., Sitko M., 2002, ApJ, 568, 1008
Cameron A. G. W., Truran J. W., 1977, Icarus, 30, 447
Chevalier R. A., 2000, ApJ, 538, L151
Clarke C. J., Pringle J. E., 1993, MNRAS, 261, 190
Dale J. E., Ercolano B., Bonnell I. A., 2012, MNRAS, 424, 377
Davis S. F., 1984, J. Comput. Phys., 56, 65
de Geus E. J., 1992, A&A, 262, 258
De Looze I., Barlow M. J., Swinyard B. M., Rho J., Gomez H. L., Matsuura M., Wesson R., 2017, MNRAS, 465, 3309
Diehl R. et al., 2006, Nature, 439, 45
Elmegreen B. G., 2000, ApJ, 530, 277
Falle S. A. E. G., 1991, MNRAS, 250, 581
Falle S., 2005, in Plewa T., Linde T., Weirs V. G. eds, Lecture Notes In Computational Science And Engineering, Vol. 41, Adaptive Mesh Refinement – Theory And Applications. Springer-Verlag, Berlin, p. 235
Foster P. N., Boss A. P., 1996, ApJ, 468, 784
Gaidos E., Krot A. N., Williams J. P., Raymond S. N., 2009, ApJ, 696, 1854
Garcia P. J. V., 2011, Physical Processes in Circumstellar Disks around Young Stars. Univ. Chicago Press, Chicago, IL
Goodson M. D., Luebbers I., Heitsch F., Frazer C. C., 2016, MNRAS, 462, 2777
Gounelle M., Meynet G., 2012, A&A, 545, A4
Gounelle M., Shu F. H., Shang H., Glassgold A. E., Rehm K. E., Lee T., 2006, ApJ, 640, 1163
Gressel O., Nelson R. P., Turner N. J., Ziegler U., 2013, ApJ, 779, 59
Hahn O., Teyssier R., Carollo C. M., 2010, MNRAS, 405, 274
Haisch K. E., Jr, Lada E. A., Lada C. J., 2001, ApJ, 553, L153
Hartmann L., 2005, in Krot A. N., Scott E. R. D., Reipurth B., eds, ASP Conf. Ser. Vol. 341, Chondrites and the Protoplanetary Disk. Astron. Soc. Pac., San Francisco, p. 131
Hartquist T. W., Dyson J. E., Pettini M., Smith L. J., 1986, MNRAS, 221, 715
Henney W. J., Arthur S. J., 1997, in Reipurth B., Bertout C., eds, Proc. IAU Symp. 182, Herbig-Haro Flows and the Birth of Stars. Kluwer, Dodrecht, p. 561
Henney W. J., O'Dell C. R., 1999, AJ, 118, 2350
Hernández J. et al., 2007, ApJ, 662, 1067
Hester J. J., Desch S. J., 2005, in Krot A. N., Scott E. R. D., Reipurth B., eds, ASP Conf. Ser. Vol. 341, Chondrites and the Protoplanetary Disk. Astron. Soc. Pac., San Francisco, p. 107
Hillenbrand L. A., Hartmann L. W., 1998, ApJ, 492, 540
Hopkins P. F., 2015, MNRAS, 450, 53
Jáchym P., Köppen J., Palouš J., Combes F., 2009, A&A, 500, 693
Jacobsen S. B., 2005, in Krot A. N., Scott E. R. D., Reipurth B., eds, ASP Conf. Ser. Vol. 341, Chondrites and the Protoplanetary Disk. Astron. Soc. Pac., San Francisco, p. 548
Jeffries R. D., Littlefair S. P., Naylor T., Mayne N. J., 2011, MNRAS, 418, 1948
Johnstone D., Hollenbach D., Bally J., 1998, ApJ, 499, 758
Kuffmeier M., Frostholm Mogensen T., Haugbølle T., Bizzarro M., Nordlund Å., 2016, ApJ, 826, 22
Lada C. J., Lada E. A., 2003, ARA&A, 41, 57
Lee T., Shu F. H., Shang H., Glassgold A. E., Rehm K. E., 1998, ApJ, 506, 898
Li S., Frank A., Blackman E. G., 2014, MNRAS, 444, 2884
Limongi M., Chieffi A., 2006, ApJ, 647, 483
Lodders K., 2003, ApJ, 591, 1220
Looney L. W., Tobin J. J., Fields B. D., 2006, ApJ, 652, 1755
McCaughrean M. J., 2001, in Schilizzi R. T., ed., Proc. IAU Symp. 205, Galaxies and their Constituents at the Highest Angular Resolutions. Kluwer, Dordrecht, p. 236
McCaughrean M. J., O'dell C. R., 1996, AJ, 111, 1977
Mann R. K., Williams J. P., 2009, ApJ, 694, L36
Mann R. K., Williams J. P., 2010, ApJ, 725, 430
Mann R. K. et al., 2014, ApJ, 784, 82
Mann R. K., Andrews S. M., Eisner J. A., Williams J. P., Meyer M. R., Di Francesco J., Carpenter J. M., Johnstone D., 2015, ApJ, 802, 77
Matzner C. D., McKee C. F., 1999, ApJ, 510, 379
Micelotta E. R., Dwek E., Slavin J. D., 2016, A&A, 590, A65
Mishra R. K., Goswami J. N., 2014, Geochim. Cosmochim. Acta, 132, 440
Nulsen P. E. J., 1982, MNRAS, 198, 1007
O'dell C. R., Wen Z., 1994, ApJ, 436, 194
O'dell C. R., Wen Z., Hu X., 1993, ApJ, 410, 696
Ogliore R. C., Huss G. R., Nagashima K., 2011, Nucl. Instrum. Meth. Phys. Res. B, 269, 1910
Ouellette N., Desch S. J., Hester J. J., Leshin L. A., 2005, in Krot A. N., Scott E. R. D., Reipurth B., eds, ASP Conf. Ser. Vol. 341, Chondrites and the Protoplanetary Disk. Astron. Soc. Pac., San Francisco, p. 527
Ouellette N., Desch S. J., Hester J. J., 2007, ApJ, 662, 1268
Ouellette N., Desch S. J., Hester J. J., 2010, ApJ, 711, 597
Pan L., Desch S. J., Scannapieco E., Timmes F. X., 2012, ApJ, 756, 102
Pittard J. M., Parkin E. R., 2016, MNRAS, 457, 4470
Povich M. S., Townsley L. K., Robitaille T. P., Broos P. S., Orbin W. T., King R. R., Naylor T., Whitney B. A., 2016, ApJ, 825, 125
Quitté G., Latkoczy C., Halliday A. N., Schönbächler M., Günther D., 2005, in Mackwell S., Stansbery E., eds, Lunar and Planetary Science XXXVI. Lunar Planet. Inst., Houston, No. 1827
Ricci L., Robberto M., Soderblom D. R., 2008, AJ, 136, 2136
Richert A. J. W., Feigelson E. D., Getman K. V., Kuhn M. A., 2015, ApJ, 811, 10
Richling S., Yorke H. W., 2000, ApJ, 539, 258
Roediger E., Brüggen M., 2006, MNRAS, 369, 567
Roediger E., Brüggen M., 2007, MNRAS, 380, 1399
Rugel G. et al., 2009, Phys. Rev. Lett., 103, 072502
Scally A., Clarke C., 2001, MNRAS, 325, 449
Shu F., Najita J., Galli D., Ostriker E., Lizano S., 1993, in Levy E. H., Lunine J. I., eds, Protostars and Planets III. Univ. Arizona Press, Tuscon, p. 3
Smith N., Bally J., Licht D., Walawender J., 2005, AJ, 129, 382
Soderblom D. R., Hillenbrand L. A., Jeffries R. D., Mamajek E. E., Naylor T., 2014, Protostars and Planets VI. Univ. Arizona Press, Tuscon, p. 219
Stapelfeldt K., Sahai R., Werner M., Trauger J., 1997, in Soderblom D., ed., ASP Conf. Ser. Vol. 119, Planets Beyond the Solar System and the Next Generation of Space Missions. Astron. soc. Pac., San Francisco, p. 131
Störzer H., Hollenbach D., 1999, ApJ, 515, 669
Tachibana S., Huss G. R., Kita N. T., Shimoda G., Morishita Y., 2006, ApJ, 639, L87
Takeuchi T., Miyama S. M., Lin D. N. C., 1996, ApJ, 460, 832
Tang H., Dauphas N., 2012, Earth Planet. Sci. Lett., 359, 248
Tassis K., Mouschovias T. C., 2004, ApJ, 616, 283
Tonnesen S., Bryan G. L., 2009, ApJ, 694, 789
Vanhala H. A. T., Cameron A. G. W., 1998, ApJ, 508, 291
Vasileiadis A., Nordlund Å., Bizzarro M., 2013, ApJ, 769, L8
Woosley S. E., Weaver T. A., 1995, ApJS, 101, 181
Young E. D., 2016, ApJ, 826, 129

This paper has been typeset from a TEX/LATEX file prepared by the author.